Defect induced structural inhomogeneity, ultraviolet light emission and near-band-edge photoluminescence broadening in degenerate In_2O_3 nanowires

Souvik Mukherjee,[1,5] Ketaki Sarkar,[1] Gary P. Wiederrecht,[4] Richard D Schaller,[4] David J Gosztola,[4] Michael A Stroscio[1,2,3] and Mitra Dutta[1,2,5]

[1] Department of Electrical and Computer Engineering, University of Illinois at Chicago, 851 South Morgan Street, M/C 154, Chicago, IL 60607, United States of America.

[2] Department of Physics, University of Illinois at Chicago, 845 W Taylor St. (M/C 273), Chicago, IL 60607, United States of America.

[3] Department of Bioengineering, University of Illinois at Chicago, 851 South Morgan Street (SEO 218), Chicago, IL 60607, United States of America.

[4] Center for Nanoscale Materials, Argonne National Laboratory, 9700 Cass Ave, Lemont, IL 60439, United States of America.

[5] E-mail: smukhe8@uic.edu and dutta@uic.edu

Abstract

We demonstrate here defect induced changes on the morphology and surface properties of indium oxide (In_2O_3) nanowires and further study their effects on the near-band-edge (NBE) emission, thereby showing the significant influence of surface states on In_2O_3 nanostructure based device characteristics for potential optoelectronic applications. In_2O_3 nanowires with cubic crystal structure (c-In_2O_3) were synthesized via carbothermal reduction technique using a gold-catalyst-assisted vapor-liquid-solid (VLS) method. Onset of strong optical absorption could be observed at energies greater than 3.5 eV consistent with highly n-type characteristics due to unintentional doping from oxygen vacancy (V_O) defects as confirmed using Raman spectroscopy. A combination of high resolution transmission electron microscopy (HRTEM), x-ray photoelectron spectroscopy (XPS) and valence band analysis on the nanowire morphology and stoichiometry reveals presence of high-density of V_O defects on the surface of the nanowires. As a result, chemisorbed oxygen species can be observed leading to upward band bending at the surface which corresponds to a smaller valence band offset (VBO) of 2.15 eV. Temperature dependent photoluminescence (PL) spectroscopy was used to study the nature of the defect states and the influence of the surface states on the electronic band structure and NBE emission has been discussed. Our data reveals significant broadening of the NBE PL peak consistent with impurity band broadening leading to band-tailing effect from heavy doping.

Keywords: Indium oxide, nanowires, carbothermal reduction, vapor-liquid-solid method, defects, photoelectron spectroscopy, Raman spectroscopy, photoluminescence, near-band-edge emission, degenerate, band tailing.

1. Introduction

Oxide semiconductor nanostructures are well known due to their novel physical, chemical and optoelectronic properties which finds applications in areas including nanoelectronics, sensing and nanophotonics. Among oxide materials, In_2O_3 nanostructures have been found to be an interesting candidate for a variety of technological applications including transparent conducting oxides (TCO) [1-3], gas sensors [4], light-emitting devices [5] and field-emission devices [6]. However, unlike other oxides, the nature of the electronic band structure (direct or indirect) and energy gap values (2.9 – 3.75 eV) in In_2O_3 are not well understood [7]. Also, contrary to the surfaces of the closely related materials such as ZnO and SnO_2, the surfaces of In_2O_3 have been studied to a much lesser extent by means of electronic structure calculations. Further, the variations in morphology and stoichiometry exhibited by the surfaces as a function of the growth environment are not well understood [8]. Most of the efforts have been focused on optimizing the material fabrication and studying the electrical properties while analysis on the role of surface states on the optical properties of In_2O_3 nanostructures and especially their NBE emission

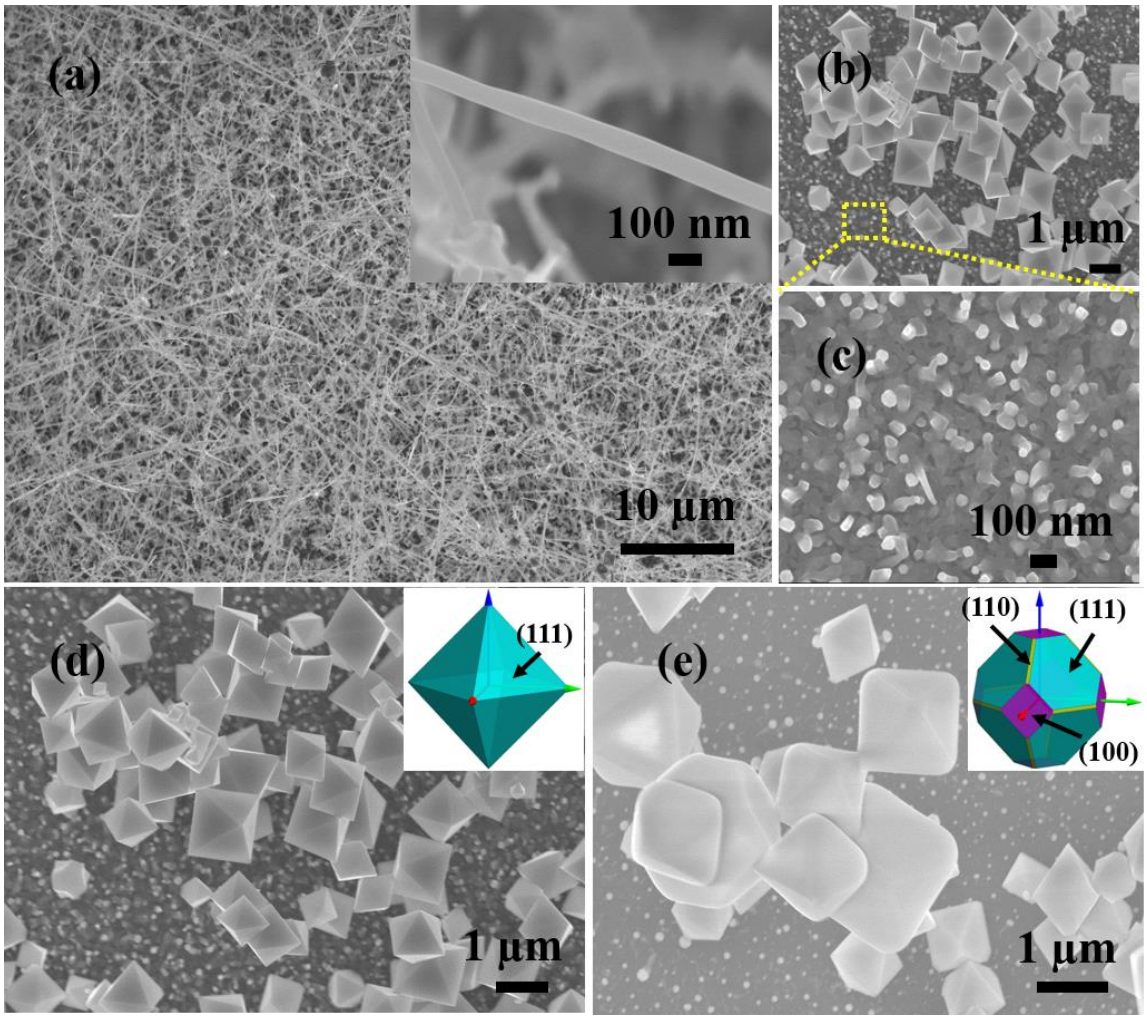

Figure 1. FE-SEM images of (a) unordered In_2O_3 nanowire mesh grown on Si substrate, inset in (a) shows corresponding high magnification image of a single In_2O_3 nanowire with diameter of ~100 nm, (b), (c) growth of nanoparticles and truncation of one-dimensional growth occurs while using indium metal source as precursor, (d), (e) perfect octahedrons and truncated octahedrons like structures, inset in (d) and (e) shows corresponding computed Wulff shapes where the planes (110), (100) and (111) are represented with colors yellow, purple and cyan respectively.

characteristics have been rarely investigated. The present work is aimed to address this deficiency and a comprehensive analysis based on experimental observations has been reported.

Most of the band gap values for In_2O_3 as reported in the literature were obtained either by transmittance or optical absorption measurements. In_2O_3 has strong optical absorption in the ultraviolet (UV) region (~3.75 eV) which has been widely interpreted as a direct band gap [9], until recently a revised fundamental gap of ~2.67 eV has been revealed through first-principles calculations and XPS measurements [10,11]. Presence of a pronounced indirect fundamental gap in In_2O_3 has also been challenged and recent reports have proposed either the presence of a parity forbidden direct gap or an indirect gap with valence band maxima (VBM) away from the Γ-point by only 50 meV [12] and is still being controversially discussed. In_2O_3 crystal structure can form cubic (c-In_2O_3), hexagonal (h-In_2O_3) and rhombohedral (rh-In_2O_3) type depending on the nature of precursor being used as well as growth conditions [13]. The cubic crystalline phase is found to be the most stable and commonly occurring [12]. Due to cubic crystal structure of In_2O_3, growth of anisotropic nanostructures such as nanowires becomes challenging, as the surface energy difference among {100}, {110} and {111} facets are minimal [14]. Variation

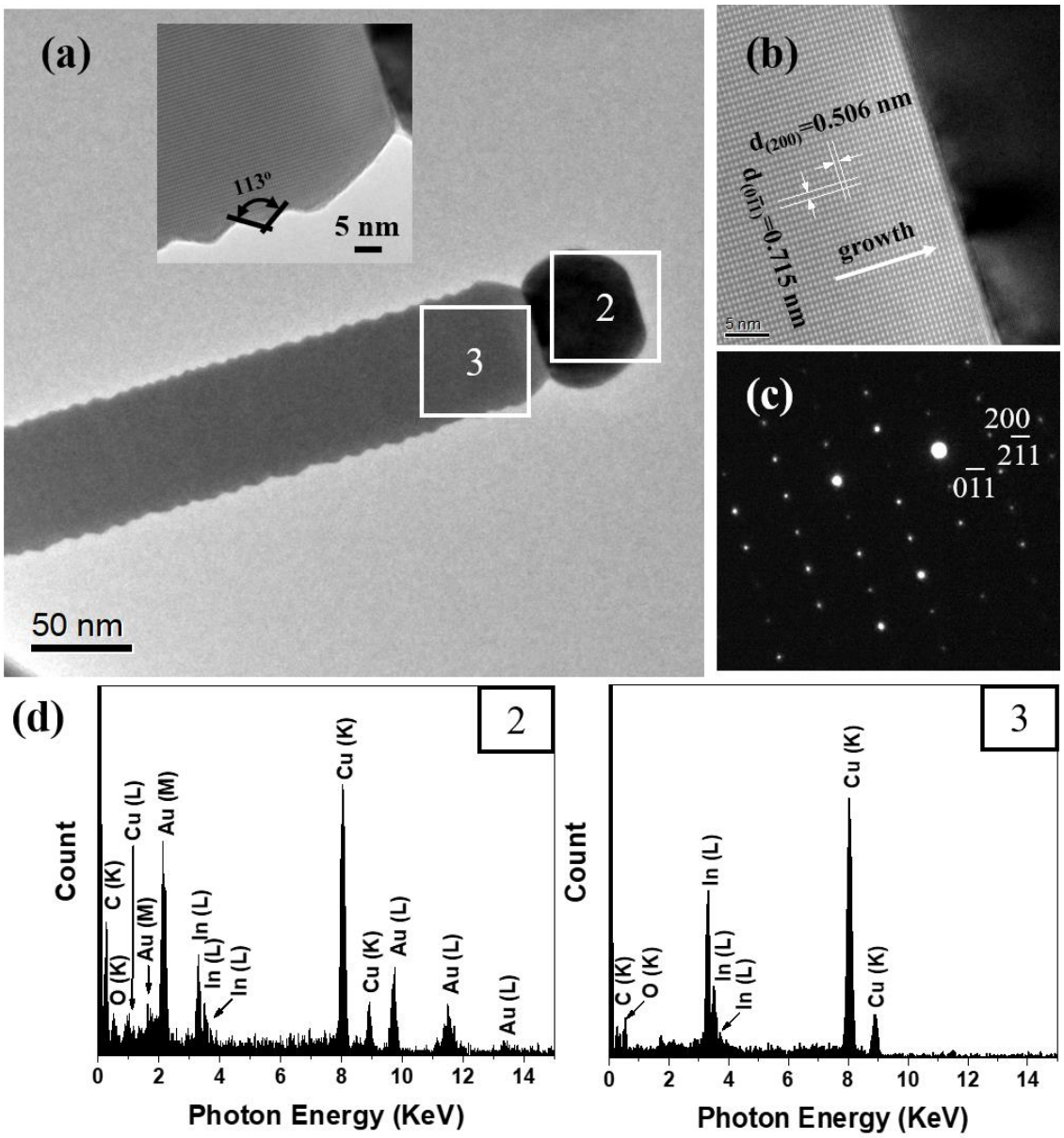

Figure 2. (a) TEM image of a single In_2O_3 nanowire, inset shows surface roughness. (b), (c) HRTEM image and SAED pattern of In_2O_3 nanowires which reveals growth along [100] direction and single crystalline properties with cubic crystal structure. (d) EDX spectrum shows elemental constituents at and below the tip of the nanowire.

in growth environment and associated process parameters such as source and deposition zone temperatures, oxygen partial pressure, carrier gas flow rate, introduction of catalyst, etc. can create significant structural defects in In_2O_3 which can alter the surface energies of various crystallographic planes [14]. This can modify the external morphology and hence the properties of the formed In_2O_3 nanostructures, thereby forming the basis for their broad range of applications [6]. Understanding the nanostructure morphology, nature of the surface states and their influence on the electronic band structure and hence on the NBE characteristics are the key factors to optimize device performance fabricated from these nanostructures for various optoelectronic applications.

2. Experimental details

In_2O_3 nanowires were synthesized on silicon substrates coated with ~3 nm Au catalyst deposited using e-beam evaporation. A mixture of In_2O_3 and graphite at a weight ratio of 4:1 was used as a source to prepare the In_2O_3 nanowires. The mixture was then transferred into a ceramic boat and placed inside a 2'' diameter quartz tube in a single zone furnace. The boat was positioned in the center of the quartz furnace tube and the Au coated Si substrate with <100> crystal orientation was placed downstream from the mixed powders. The source was heated up to 950 ºC in about 35 mins and the temperature of the deposition zone was adjusted by varying the distance of the substrates from the source. The nanowire growth was carried out at a deposition zone temperature of 900 ºC which is ~6 cm downstream from the center of the furnace for 45-50 min duration at a constant flow of 300 sccm of argon as a carrier gas. Nanoparticles with octahedron like morphologies were synthesized using indium metal shots of 2-5 mm diameter as the source. The nanoparticle growth was performed at a higher deposition zone temperature of 950 ºC with the substrates placed adjacent to the source boat at the center of the furnace. The growth duration was varied in between 30-60 min keeping other experimental conditions same as that used during the nanowire growth. Low resolution images of randomly assembled nanostructures were obtained using a JEOL JSM7500F field emission scanning electron microscope (FE-SEM). HRTEM images of the nanostructures were obtained using a JEOL JEM 3010 electron microscope. XPS measurements were performed using a Kratos AXIS-165 spectrometer equipped with a monochromatic Al Kα source (1486.6 eV). The spectrometer take off angle was zero with respect to the sample surface and the pass energy was 20 eV with a step size of 0.1 eV. Optical properties were investigated using Raman spectroscopy using Renishaw inVia Confocal Microscope with 633 nm non-resonant and 325 nm resonant excitation wavelengths, photoluminescence spectroscopy at room temperature with 290 nm excitation from a xenon lamp and collected using Horiba Jobin-Yvon Nanolog Spectrofluorimeter while low temperature PL investigation was done in a closed cycle helium cryostat capable of reaching down to 10 K. All experiments were repeated over multiple samples for reproducibility.

3. Results and discussion

3.1. In_2O_3 nanowires: growth and morphology

Figure 1(a) shows SEM image of a dense mesh of In_2O_3 nanowires synthesized via the carbothermal reduction technique. In_2O_3 powder couldn't evaporate by itself due to its very high melting point (1910 ºC). As a result, there are intermediate reaction steps involved at both the source and deposition sites. Redox reactions at the source generate In_2O(v) which possesses a very high vapor pressure and is transported downstream to the Au coated silicon substrates where it gets absorbed by the Au-catalytic droplets and decomposes to In(l) and In_2O_3(s). The In(l) further reacts with Au clusters to form an Au-In eutectic which becomes the preferred absorption site for incoming In_2O(v). Supersaturation of the eutectic results in the precipitation of In(s) at the liquid-solid interface where it reacts with oxygen to form In_2O_3(s). Au-catalyst assisted one-dimensional growth continues as long as there is sufficient supply of In_2O(v). The possible reactions steps can be described by the following [15]:

$$In_2O_3(s) + C(s) \rightarrow In_2O(v) + CO_2(v) \quad (1)$$

$$3In_2O(v) \rightarrow 4In(l) + In_2O_3(s) \quad (2)$$

$$In(l) + \frac{3}{2}O_2(g) \rightarrow In_2O_3(s) \quad (3)$$

The nanowires were found to have an average diameter of ~100 nm as shown in the inset of figure 1(a). Attempts to grow In_2O_3 nanowires by directly heating an indium metal source was not successful. From figure 1(b) and figure 1(c), we observe that the one-dimensional growth appears to have stopped intermittently. This might be due to high supersaturation ratio of oxidized indium vapor which essentially facilitates the growth of nanoparticle like structures [14]. The computed Wulff shape based on the ratio of growth rate (r) perpendicular to different low-index crystallographic planes reveals perfect octahedron formation when $r_{\{100\}}:r_{\{111\}} \approx 1.73$ as shown in figure 1(d). We also observed truncated octahedron like features shown in figure 1(e) which could be due to environmental disturbances inside the quartz tube. Formation of these structures corresponds to $r_{\{110\}}:r_{\{100\}}:r_{\{111\}}$

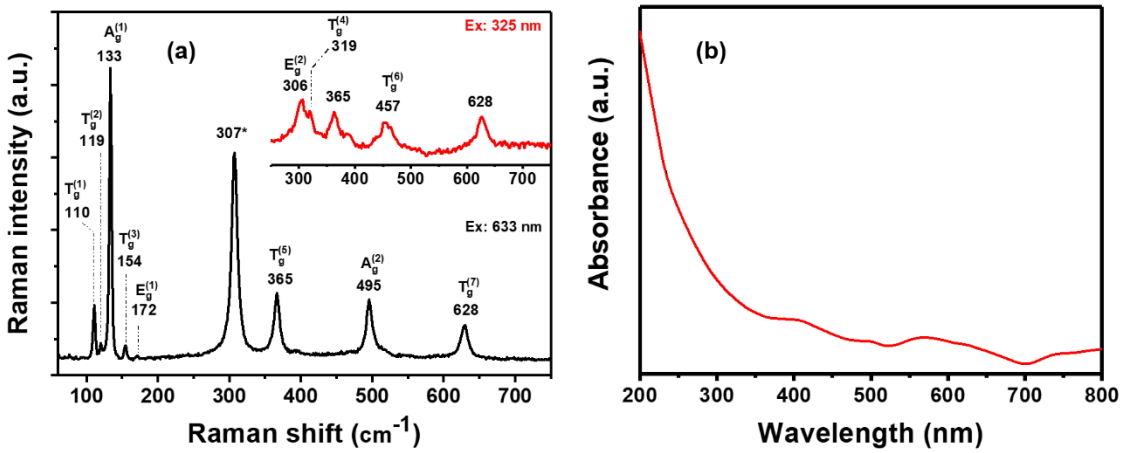

Figure 3. (a) Room temperature non-resonant Raman spectra of In_2O_3 nanowires showing significant broadening of phonon mode at 307 cm^{-1} associated with V_O defects present in the crystal lattice (inset shows corresponding resonant Raman spectra). (b) UV-Visible absorption spectra of In2O3 nanowires.

≈ 1.2:1.2:1, which agrees well with the experimental observations and with literature reports [14,16]. Unlike the growth of uniform diameter nanowires, the size of the nanoparticles with octahedron like morphologies varied considerably ranging from 200 nm to 1.5 µm in diameter. This variation in the size of the nanoparticles could be due to their uncontrolled growth from self-catalytic nucleation sites as no evidence of Au catalyst was found from corresponding elemental characterization as shown in figure S2(c).

HRTEM, selected area electron diffraction (SAED) and energy-dispersive x-ray (EDX) characterization were performed on individual In_2O_3 nanowires to gain insight regarding the nanowire morphology and the representative results are shown in figure 2. The nanowires were found to be single crystalline in nature with body-centered cubic (bcc) crystal structure as observed from the HRTEM and corresponding SAED images shown in figure 2(b)-2(c). The interplanar spacing of the lattice fringes along the longitudinal and transverse directions was measured to be 0.506 nm and 0.715 nm which correspond to (200) and $(0\bar{1}1)$ planes respectively. From the SAED patterns and lattice images, the growth direction was determined to be along [100]. Point EDX measurements performed at two different sites on a single nanowire as numerically labeled in figure 2(d), reveals that the tip of the nanowire is rich in Au-In, thereby confirming the nanowires have grown following the Au-catalytic VLS route as discussed earlier. HRTEM images taken at the edge of the nanowires reveals a rugged morphology on the nanoscale where the angle between the two consecutive edge planes was determined to be ~113° and appears to be symmetric with respect to the edge normal as shown in the inset of figure 2(a). Since the inclusion angle between (100) and (111) planes is 54.7°, the edges are believed to be {111} planes and has been previously reported by Jean *et al.* [15] which was observed during In_2O_3 nanotower formation.

3.2. Structural characterization: quality of the as-synthesized In_2O_3 nanowires

Raman spectroscopy analysis was carried out at room temperature to study the crystal quality of the In_2O_3 nanowires as shown in figure 3(a). From the Raman spectrum, we see in total 11 modes of A_g, E_g and T_g symmetry that are ascribed to typical modes in c-In_2O_3. Phonon modes having weak scattering intensities however can be expected to be visible with resonant excitation as shown in the inset of figure 3(a), where the phonon mode at 307 cm^{-1} is resolved into two constituent modes of E_g (306 cm^{-1}) and T_g (319 cm^{-1}) symmetry respectively. However, with resonant excitation, a significant fluorescence background was present and needed to be subtracted which resulted in the overall spectra to appear noisier. Defects of any kind if introduced to the crystal which could be a result of disorder, doping, or impurities, will likely bring a breakdown of the usual $\vec{q} = 0$ selection rule, thus creating broadening and asymmetry to the Raman line shape. We observe significant

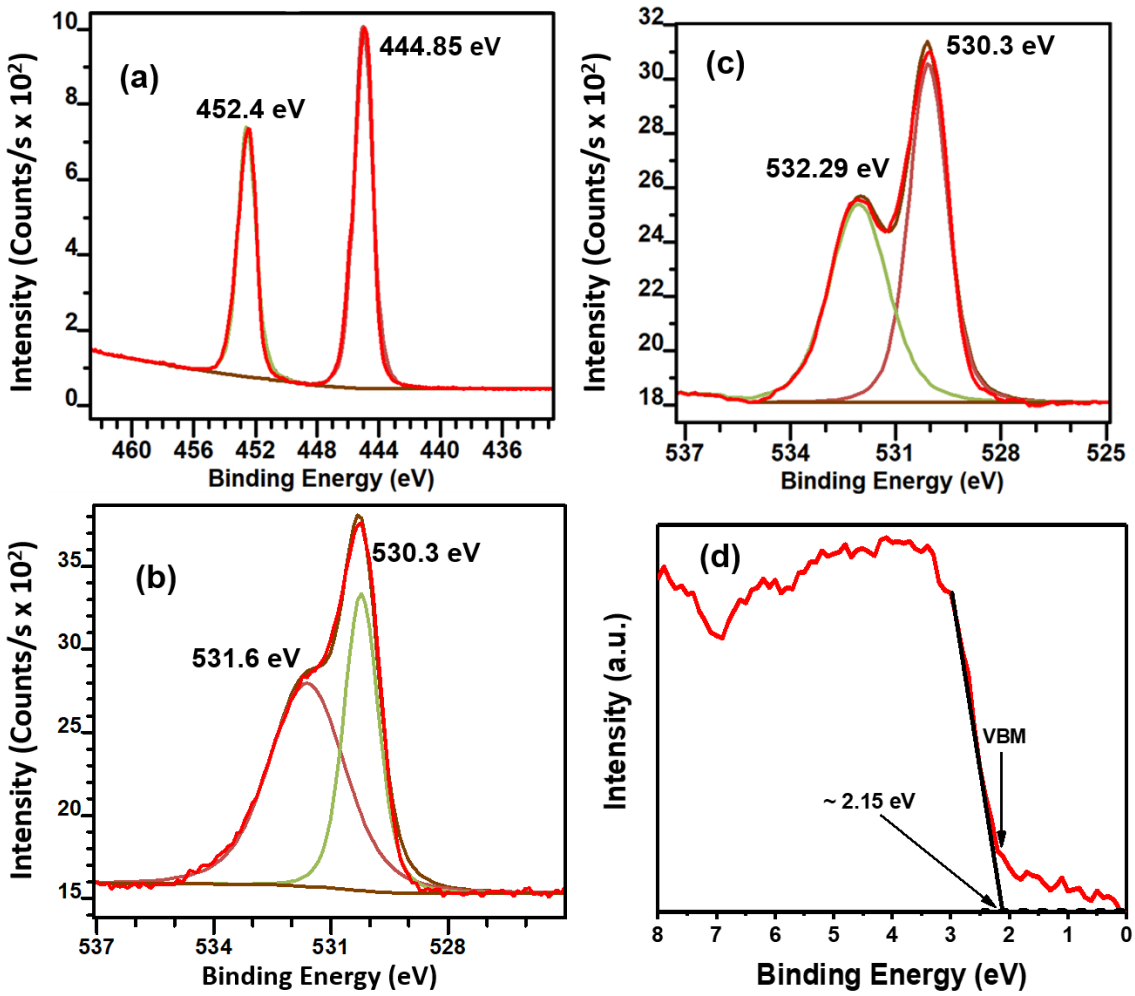

Figure 4. High resolution XPS spectrum of (a)-(c) In (3d) and O(1s). O(1s) spectrum in figure 4(b) and 4(c) shows presence of a minor second peak at higher binding energy associated with chemisorbed oxygen species on the surface of the nanowires. (d) XPS valence band photoemission spectra of In_2O_3 nanowires.

broadening of the phonon mode centered at 307 cm^{-1} having an FWHM of ~12 cm^{-1}. This mode corresponds to the stretching mode in In_2O_3 and is very sensitive to oxygen vacancies [6]. V_O defects are expected to be present in very high concentration because of significantly lower formation energies [12] and correlates well with our absorption measurements. Comprehensive optical analysis has revealed that strong optical transitions occur only from ~0.8 eV below the top of the valence band [10]. From optical absorption measurements as shown in figure 3(b), we observed the onset of strong absorption at energies between 3.5-3.75 eV. However, a well-defined value of the optical gap could not be ascertained by analyzing a long-section wavelength of the absorption edge. The observed characteristic could arise due to the presence of additional energy states near the conduction band edge because of V_O defects formed mostly on the surface of the nanowires [7]. These surface states can trap electrons from the valence band and make a contribution to the absorption. Unintentional doping because of V_O defects results in an n-type characteristic as two free electrons are added to the crystal lattice every time a vacancy is created. High density of V_O defects thereby may shift the Fermi level close to the conduction band edge resulting in the In_2O_3 nanowires to become highly n-type semiconductor.

3.3. In_2O_3 nanowire surface modification through faceting and chemisorption

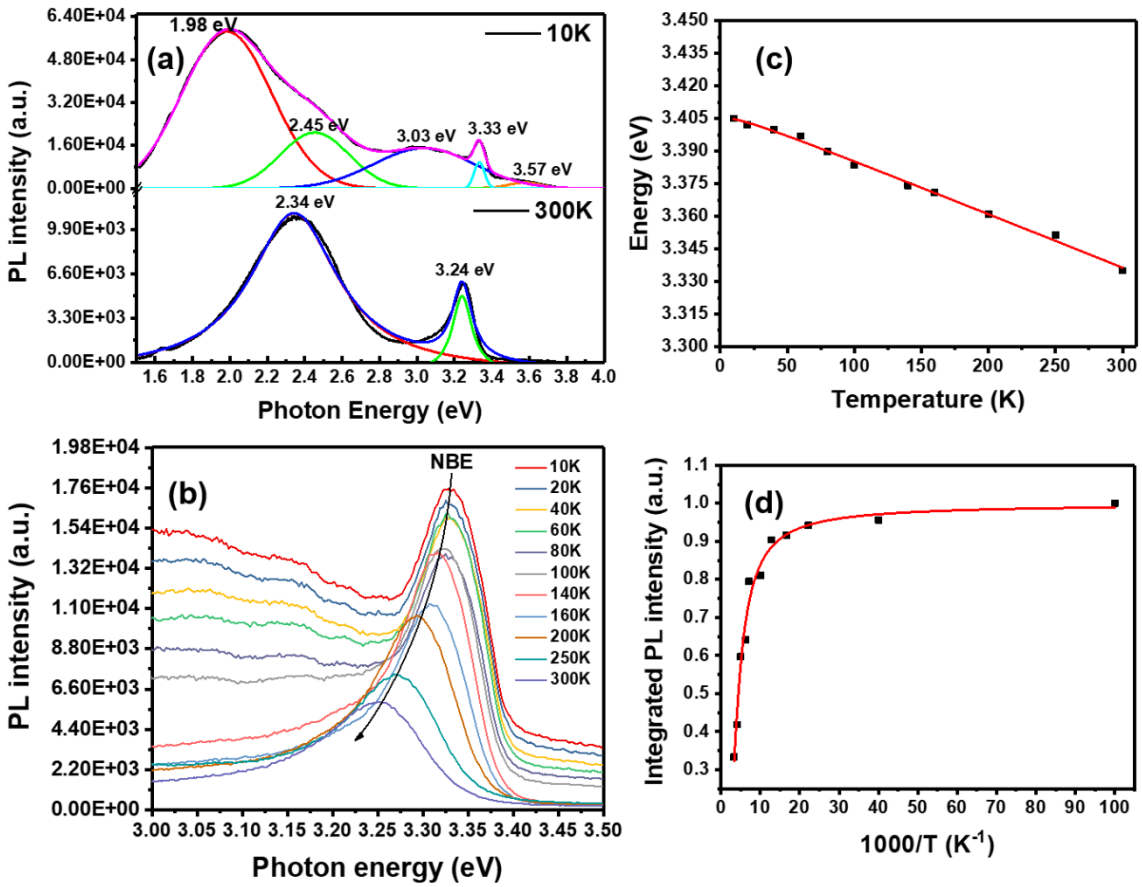

Figure 5. (a) Low (10 K) and room temperature PL spectra fitted with multiple Gaussian peaks identifying corresponding transition energies. (b) Temperature dependent NBE PL spectra. (c) Temperature dependence of the high energy edge of the NBE peak. (d) Thermal quenching behavior of NBE peak.

It is well known that stabilization of surfaces with a resultant non-zero dipole moment perpendicular to the surface occurs through rearrangement of surface charges or through introduction of compensating charges into the outermost surface planes. Such reconstruction can significantly affect the surface geometric structure as well as stoichiometry and often has been associated with surface roughening or adsorption of foreign atoms [17]. The bcc-structure of In_2O_3 is related to a 2 × 2 × 2 supercell of fluorite and its bixbyite surfaces are very similar in appearance to those of the parent fluorite structure [12]. The (001) surface of fluorite is a "Type III" ionic surface within the Tasker classification and contains alternating cation and anion planes thereby giving rise to a surface dipole. This may be stabilized in a simple manner through faceting [18] as can be observed in figure 2(a) where (111) facets have formed, which is the overall most stable surface of c-In_2O_3 followed by the (011) surfaces. The (111) surface is highly sensitive to oxygen chemical potential. As a result, V_O defects can easily form on the surface compared to the bulk which might result in chemisorption of oxygen species on the In_2O_3 surface as well as band bending effects due to surface states [19].

High resolution XPS measurements were performed and the binding energies were corrected with respect to the well-known C(1s) peak at 284.6 eV. The In $3d_{5/2}$ peak and O(1s) peak are observed at 444.85 eV and 530.3 eV respectively, suggesting that the major constituent phase is In_2O_3. Background subtraction was performed using the Touggard function. The atomic concentration of indium and oxygen were calculated to be 33% and 67% respectively providing evidence of a significant amount of chemisorbed oxygen species on the surface. The asymmetric O(1s) peak shown in figure 4(b) was deconvoluted using a Gaussian function and a reasonably good

fit with the experimental data was obtained. Two peaks were required to fit the measured O(1s) spectra with resolved peak positions at 530.3 eV and 531.6 eV respectively. In figure 1(b), the feature at 530.3 eV is the lattice oxygen O^{2-} on the surface whereas the feature at 531.6 eV is believed to be from chemisorbed oxygen species [20, 21]. Occasionally we also observed a minor peak at 532.29 eV as shown in figure 4(c) due to the hydroxyl and/or oxy-hydroxyl oxygen species, possibly from water as the (111) and (011) surfaces in In_2O_3 are known to adsorb water and promote dissociation of molecules [8]. At high temperatures (> 200 ºC), oxygen molecules dissociate into atomic form which can reside on the surface either as neutral $O_{(ads)}$ or charged $O^{-}_{(ads)}$ upon trapping an electron from the semiconductor [21]. Due to adsorbed species on the surface of the In_2O_3 nanowires, the surface Fermi level can vary by up to 1.5 eV depending on the sample preparation [22]. It is known that the combination of core level and valence band XPS constitutes a useful method of determining VBOs in a rather direct fashion. The VBM to surface Fermi level separation was determined to be 2.15 ± 0.2 eV as shown in figure 4(d) based on the linear method [22]. The value obtained for VBO is smaller compared to values reported in the literature mostly for thin-film samples [23] and could be attributed to upward band-bending due to negatively charged oxygen species residing on the surface. This puts the surface Fermi level below the conduction band minima (CBM) which makes the surface less n-type. The carrier concentration (n) is given by [24]

$$n = 2\left[\frac{2\pi m_e^* K_B T}{h^2}\right]^{\frac{3}{2}} exp\left(\frac{E_F - E_C}{K_B T}\right) \qquad (4)$$

where $m_e^* = 0.3\, m_0$ [12] is the effective electron mass. Taking T = 300 K, the net electron concentration at the surface was estimated to be 1.65 x 10^{15} cm^{-3}. Hence, our XPS measurements confirm the presence of a high-density of V_O defects on the surface of the nanowires. Depending on the nature of the surface states in nanostructures, a profound influence on the optoelectronic properties [19,25] can be observed. This has been further investigated using temperature dependent PL spectroscopy and its influence on the emission characteristics of as-synthesized In_2O_3 nanowires has been discussed.

3.4. Identification of defect states and their influence on the NBE emission characteristics of In_2O_3 *nanowires*

Figure 5(a) shows the PL spectrum in an extended wavelength range taken at 10 K and at room temperature. Both spectra show strong UV emission but an even stronger peak in the visible part of the spectrum can be observed. Let's first focus on the observed UV emission from In_2O_3 nanowires at room temperature which has been rarely reported [5,7,26]. It is interesting to note that the observed NBE peak centered at 3.24 eV at room temperature is a broad peak with FWHM of ~160 meV and does not get resolved into expected narrow emission peaks even at very low temperatures as can be observed from the 10 K spectra. To the best of our knowledge, this type of observation has not been reported before for In_2O_3. The origin of the NBE peak is believed to be from a series of shallow donor levels formed due to neutral oxygen vacancy (V_O^X) defects present on the surface of the nanowires [7]. Broadened NBE emission with no excitonic emission features even at very low temperatures is clearly an indication of very high doping which causes the discrete shallow donor levels to merge into an impurity band. The feature at 3.57 eV arises due to the presence of a weak fluorescence background signal from the quartz coverslip on which the nanowires were transferred for low temperature photoluminescence measurements. Control measurements were performed on the substrate and subtracted from the overall spectra that does correct most if not all the background features which can be due to experimental fluctuations. In the experimental setup, we have utilized a 320 nm long pass filter to block the tail of the 290 nm excitation. The effect of the filter can be observed from the 10 K spectra in figure 5(a) where the background signal at ~3.8 eV (320 nm) and higher energies goes down to zero whereas at energies lower than 3.8 eV, a weak fluorescence from the substrate persists creating an impression of a broad Gaussian peak like feature. The fitting function identifies this feature as an additional peak while performing deconvolution of the overall spectra to extract individual components and associated peak positions.

Figure 5(b) shows the temperature dependent PL spectrum (10 K – 300 K) of the NBE peak. The intensity of the broad NBE peak decreases progressively with increasing temperature and shows a characteristic red-shift of 90 meV at room temperature relative to the 10 K spectra and merges into a broader peak possibly due to phonon

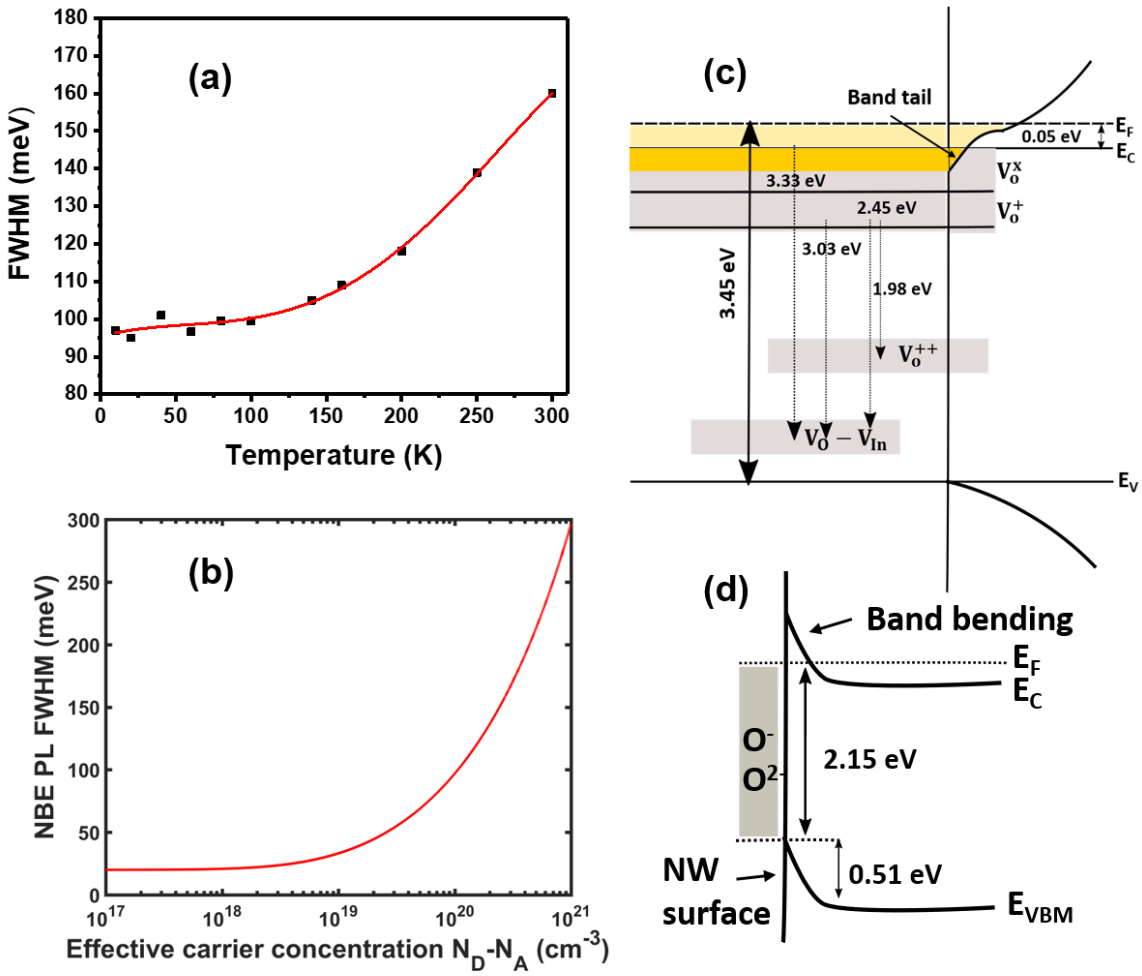

Figure 6. (a) Dependence of NBE peak FWHM on temperature. (b) NBE PL line width as a function of effective carrier concentration based on the impurity band broadening model. (c) Schematic band diagram of In_2O_3 nanowires showing energy transitions due to different charge states of V_O defects and band tailing effect. (d) Upward band bending on the surface due to chemisorbed oxygen species.

scattering effects. From the 10 K spectra in figure 5(a), we also observe an emission peak centered at 3.03 eV, which is below the band-edge and appears to have merged with the NBE peak at temperatures above 140 K. The below band edge peak at 3.03 eV is believed to originate from donor levels formed due to singly ionized oxygen vacancies (V_O^+). It can be observed from figure 5(c) that the high energy edge of the NBE peak defined as 1% of the peak intensity point decreases monotonically with increasing temperature and can be described by the well-known Varshni equation [27].

$$E(T) = E(0) - \frac{\alpha T^2}{T+\beta} \qquad (5)$$

where E(0) is the excitonic band gap at 0 K, and α, β are the corresponding thermal coefficients. A good fit was obtained (red curve) with the experimental data (black squares) and the value of E(0) was found to be 3.41 eV which can be considered as the lower bound of the optical gap and is in close agreement with previously reported values for highly n-type In_2O_3 nanostructures [7]. The extracted fitting parameters α = 3.507 x 10^{-4} eV/K and β = 140 ± 20 K are consistent with previously reported values by Wei *et al.* [26]. A smaller value of the thermal coefficient β which is proportional to the Debye temperature (Θ_D) [27] indicates in general poor lattice thermal conductivity of the nanowires. This is expected for highly doped semiconductors due to enhanced electron-phonon coupling resulting in higher scattering and has previously been observed for highly doped n-type

semiconductor where Θ_D was found to decrease with increasing carrier concentration [28]. From the temperature dependence of the NBE peak, we estimate the nature of the quenching channels present as shown in figure 5(d) which is described by the modified Arrhenius equation: [3]

$$I(T) = \frac{I(0)}{\left(1+A_1\, exp\left(-\frac{E_1}{K_B T}\right)+A_1\, exp\left(-\frac{E_2}{K_B T}\right)\right)} \qquad (6)$$

where, I(T) and I(0) are the PL intensities at temperature T and 10 K, respectively; E_i is the activation energy, K_B is the Boltzmann constant, and A_i is a constant. By using a two-channel fit and considering both A_1 and A_2 constants, we found E_1 and E_2 to be 6 meV and 75 meV, respectively. These correspond to effective ionization energy of donors and acceptor like states respectively. The acceptor like states may be a series of shallow oxygen-indium vacancy pairs (V_O-V_{In}) or deeper indium vacancies (V_{In}) which act as compensating centers [7] and can significantly contribute towards defect emissions from below the band-edge resulting in broad visible emission peaks centered at 2.45 eV and 1.98 eV in the 10 K PL spectra. Due to thermal ionization effects at higher temperatures, these peaks merges into a single broad peak centered at 2.34 eV as observed from the room temperature PL spectra.

The Burstein-Moss effect and impurity band broadening are the two proposed mechanisms for such modified NBE emission spectrum [29]. The Burstein-Moss effect is a result of Fermi level shift above the CBM when doping exceeds the degeneracy limit (~2.5 x 10^{19} for In_2O_3) and is frequently observed in heavily-doped semiconductors whereas impurity band broadening occurs because of potential fluctuations due to randomly distributed impurities which can cause discrete donor levels to evolve into impurity bands ultimately leading to a band tail. For heavily doped samples, the FWHM predicted by the Burstein-Moss model is expected to be significantly higher than what we observe here (~95 meV at 10 K) [29]. We also do not observe a sharp cutoff on the high energy side of the NBE peak which is the characteristic of momentum non-conserving indirect transitions [30]. Further the NBE line shape of the 10 K PL spectra exhibits a characteristic Gaussian nature in the Stoke's part of the line as evident from the fitted curve in figure 5(a) which leads us to believe that broadening of the impurity band plays a major role in the observed PL. The width of the band tails, and thus the dependence of the NBE peak line width on carrier concentration, can be calculated based on the impurity band broadening model proposed by Morgan *et al.* [31].

Figure 6(a) shows the FWHM of the NBE peak as a function of temperature, where the red curve is a guide to the eyes. V_O^X defect levels expand into a defect band which overlaps with the conduction band thereby shifting the edge to the low energy side and a band tail is formed [32]. The FWHM of the PL line width can be expressed as [29]

$$FWHM = \left[\Gamma_T{}^2 + \left(2^{\frac{3}{2}}\, ln\, 2\, \sigma_i\right)^2\right]^{3/2} \qquad (7)$$

Γ_T is the broadening due to thermal and static disorder (typical ~20 meV) and can be ignored in this case. σ is the second moment of the Gaussian-shaped potential fluctuation distribution function [29] and is given by,

$$\sigma^2 = \left[C_1 c\, n^{5/6}\, exp\left(-C_2\sqrt{\frac{2}{c+1}}\, n^{-1/4}\right)\right]^{3/2} \qquad (8)$$

where c ~ 1 is the compensation ratio, n is the net electron concentration and C_1 and C_2 are constants as derived by Ilipoulos *et al.* [33]. We thus estimate an electron concentration of 1.2 x 10^{20} cm^{-3} at 10 K and the corresponding plot of equation (7) is shown in figure 6(b). The calculated electron concentration is higher than the degeneracy limit in In_2O_3, hence the In_2O_3 nanowires were found to be degenerate with Fermi level lying ~0.05 eV above the CBM. A representative schematic of the flat-band structure, probable energy transitions and the effect of band tailing in In_2O_3 nanowires is shown in figure 6(c) whereas figure 6(d) shows representative upward band bending (~0.51 eV) on the surface of the nanowires due to presence of chemisorbed oxygen species. Absorption occurs from the valence band to the Fermi level whereas luminescence occurs from the band tail to

acceptor like states. Similar observations of remarkable PL broadening have previously been observed for n-GaN films [33] and indium doped n-type ZnO nanowires [29].

4. Conclusion

In conclusion, a detailed investigation on the defect induced changes in the In_2O_3 nanowire morphology, surface properties and NBE emission characteristics has been presented. The surface of nanowires loses many of the lattice O^{2-}, leading to the formation of oxygen vacancies which results in significant chemisorption of charged oxygen species. This causes upward band bending of 0.51 eV on the surface of In_2O_3 nanowires which results in a smaller value of VBO obtained using XPS valence band spectroscopy. Further insight on the nature of the defects and their influence on the NBE emission were obtained using temperature dependent PL spectroscopy. We observed UV emission from the band-edge and significant NBE PL line width broadening associated with formed V_O^X impurity band at the surface which merges with the conduction band forming a band tail. The optical gap was calculated to be 3.41 eV and activation energies of 6 meV and 75 meV were obtained and related to ionizing energies of donor and acceptor like defects respectively. An electron concentration of 1.2 x 10^{20} cm^{-3} at 10 K was estimated which is above the degeneracy limit of In_2O_3, hence positioning the Fermi level 0.05 eV above the CBM. We are further investigating the effect of tailoring the surface properties on carrier dynamics of these nanowires for potential application as ultrafast terahertz photonic devices.

Acknowledgement

The work at UIC was partially supported by Grant No. FA9550-15-1-0493 from the Air Force Office of Scientific Research. This work made use of instruments in the Electron Microscopy Service (Research Resources Center, UIC). Use of the Center for Nanoscale Materials, an Office of Science user facility, was supported by the U.S. Department of Energy, Office of Science, Office of Basic Energy Sciences, under Contract No. DE-AC02-06CH11357.

References

[1] Minami, T 2005 *Semicond. Sci. Technol.* **20** S35

[2] Phillips J M, Cava R J, Thomas G A, Carter S A, Kwo J, Siegrist T, Krajewski J J, Marshall J H, Peck Jr W F, Rapkine D H 1995 *Appl. Phys. Lett.* **67** 2246-8

[3] Farid S, Mukherjee S, Sarkar K, Mazouchi M, Stroscio MA, Dutta 2016 M *Appl. Phys. Lett.* **108** 021106

[4] Zhang D, Li C, Liu X, Han S, Tang T, Zhou C 2003 *Appl. Phys. Lett.* **83** 1845-7

[5] Cao H, Qiu X, Liang Y, Zhu Q, Zhao M 2003 *Appl. Phys. Lett.* **83** 761-3

[6] Hafeez M, Zhai T, Bhatti A S, Bando Y, Golberg D 2012 *Cryst. Growth Des.* **12** 4935-43

[7] Ho C H, Chan C H, Tien L C, Huang Y S 2011 *J. Phys. Chem. C* **115** 25088-96

[8] Agoston P, Albe K 2011 *Phys. Rev. B* **84** 045311

[9] King P D, Veal T D, Fuchs F, Wang C Y, Payne D J, Bourlange A, Zhang H, Bell G R, Cimalla V, Ambacher O, Egdell R G 2009 *Phys. Rev. B* **79** 205211

[10] Walsh A, Da Silva J L, Wei S H, Körber C, Klein A, Piper L F, DeMasi A, Smith K E, Panaccione G, Torelli P, Payne D J 2008 *Phys. Rev. Lett.* **100** 167402

[11] Bourlange A, Payne D J, Egdell R G, Foord J S, Edwards P P, Jones M O, Schertel A, Dobson P J, Hutchison J L 2008 *Appl. Phys. Lett.* **92** 092117

[12] Bierwagen O 2015 *Semicond. Sci. Technol.* **30** 024001

[13] Karazhanov S Z, Ravindran P, Vajeeston P, Ulyashin A, Finstad T G, Fjellvåg H 2007 *Phys. Rev. B* **76** 075129

[14] Hao Y, Meng G, Ye C, Zhang L 2005 *Cryst. Growth Des.* **5** 1617-21

[15] Jean S T, Her Y C 2010 *Cryst. Growth Des.* **10** 2104-10

[16] Yan Y G, Zhang Y, Zeng H B, Zhang L D 2007 *Cryst. Growth Des.* **7** 940-3

[17] Tasker P W 1979 *J. Phys. C* **12** 4977

[18] Egdell R G 2015 *Dopant and Defect Induced Electronic States at In2O3 Surfaces* vol 58 ed Jupille J and Thornton G (Switzerland: Springer) p 351

[19] Kar A, Stroscio M A, Dutta M, Kumari J, Meyyappan M 2009 *Appl. Phys. Lett.* **94** 101905.

[20] Nguyen P, Vaddiraju S, Meyyappan M 2006 *J. Electron. Mater.* **35** 200-6

[21] Kar A, Stroscio M A, Meyyappan M, Gosztola D J, Wiederrecht G P, Dutta M 2011 *Nanotechnology* **22** 285709.

[22] Chambers S A, Droubay T, Kaspar T C, Gutowski M 2004 *J. Vac. Sci. Technol.* **22** 2205-15

[23] Harvey S P, Mason T O, Gassenbauer Y, Schafranek R, Klein A 2006 *J. Phys. D* **39** 3959

[24] Robert F 2003 *Pierret: Semiconductor device fundamentals* (Reading, MA: Addison-Wesley)

[25] Li C, Zhang D, Lei B, Han S, Liu X, Zhou C. 2003 *J. Phys. Chem. B* **107** 12451-5.

[26] Wei Z P, Guo D L, Liu B, Chen R, Wong L M, Yang W F, Wang S J, Sun H D, Wu T 2010 *Appl. Phys. Lett.* **96** 031902

[27] Varshni Y P 1967 *Physica* **34** 149-54

[28] Baranskii P I, Elizarov A I 1972 *Phys. Status Solidi B* **53** K45-9

[29] He H P, Wang Z, Duan H F, Ye Z Z 2015 *Phys. Chem. Chem. Phys.* **17** 17552-6

[30] Yoshikawa M, Kunzer M, Wagner J, Obloh H, Schlotter P, Schmidt R, Herres N, Kaufmann U 1999 *J. Appl. Phys.* **86** 4400-2

[31] Morgan T N 1965 *Phys. Rev.* **139** A343

[32] Zhu Q, Xie C, Li H, Yang C, Zhang S, Zeng D 2014 *J. Mater. Chem. C* **2** 4566-80

[33] Iliopoulos E, Doppalapudi D, Ng H M, Moustakas T D 1998 *Appl. Phys. Lett.* **73** 375-7